AD-A193 200 THE LOW-LATITUDE AURORAL BOUNDARY: STEADY-STATE AND TIME-DEPENDENT REPRES..(U) AEROSPACE CORP EL SEGUNDO CA SPACE SCIENCES LAB D J GORNEY ET AL. 25 MAR 88 1/1

UNCLASSIFIED TR-0086(2940-06)-3 SD-TR-88-47 F/G 4/1 NL

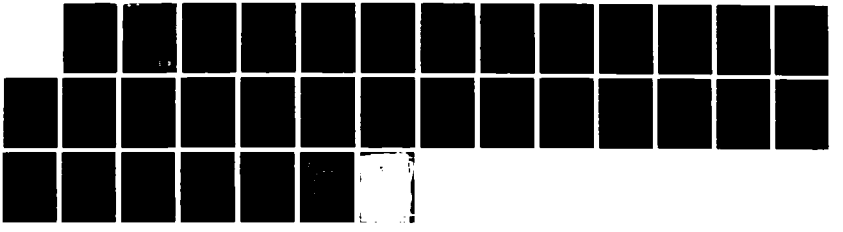

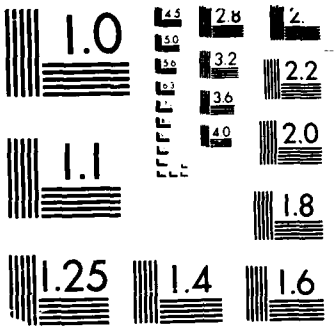

REPORT SD-TR-88-47

(4)

The Low-Latitude Auroral Boundary: Steady-State and Time-Dependent Representations

D. J. GORNEY
Space Sciences Laboratory
Laboratory Operations
The Aerospace Corporation
El Segundo, CA 90245

and

D. S. EVANS
Space Environment Laboratory
NOAA

25 March 1988

Prepared for

SPACE DIVISION
AIR FORCE SYSTEMS COMMAND
Los Angeles Air Force Base
P.O. Box 92960, Worldway Postal Center
Los Angeles, CA 90009-2960

UNCLASSIFIED

SECURITY CLASSIFICATION OF THIS PAGE

REPORT DOCUMENTATION PAGE

1a. REPORT SECURITY CLASSIFICATION Unclassified	1b. RESTRICTIVE MARKINGS
2a. SECURITY CLASSIFICATION AUTHORITY	3. DISTRIBUTION / AVAILABILITY OF REPORT Approved for public release; distribution unlimited.
2b. DECLASSIFICATION / DOWNGRADING SCHEDULE	
4. PERFORMING ORGANIZATION REPORT NUMBER(S) TR-0086(2940-06)-3	5. MONITORING ORGANIZATION REPORT NUMBER(S) SD-TR-88-47
6a. NAME OF PERFORMING ORGANIZATION The Aerospace Corporation Laboratory Operations 6b. OFFICE SYMBOL (If applicable)	7a. NAME OF MONITORING ORGANIZATION Space Division
6c. ADDRESS (City, State, and ZIP Code) El Segundo, CA 90245	7b. ADDRESS (City, State, and ZIP Code) Los Angeles Air Force Base Los Angeles, CA 90009-2960
8a. NAME OF FUNDING / SPONSORING ORGANIZATION 8b. OFFICE SYMBOL (If applicable)	9. PROCUREMENT INSTRUMENT IDENTIFICATION NUMBER F04701-85-C-0086
8c. ADDRESS (City, State, and ZIP Code)	10. SOURCE OF FUNDING NUMBERS PROGRAM ELEMENT NO. / PROJECT NO. / TASK NO / WORK UNIT ACCESSION NO.

11. TITLE (Include Security Classification)
The Low-Latitude Auroral Boundary: Steady State and Time-Dependent Representations

12. PERSONAL AUTHOR(S)
Gorney, D. J., and Evans, D. S., Space Environment Laboratory, NOAA

13a. TYPE OF REPORT	13b. TIME COVERED FROM ____ TO ____	14. DATE OF REPORT (Year, Month, Day)	15. PAGE COUNT
		1988 March 25	30

16. SUPPLEMENTARY NOTATION

17. COSATI CODES		
FIELD	GROUP	SUB-GROUP

18. SUBJECT TERMS (Continue on reverse if necessary and identify by block number)
Aurora
Magnetospheric particles
Magnetospheric activity

19. ABSTRACT (Continue on reverse if necessary and identify by block number)

Recently, extensive data sets have been acquired from charged-particle detectors on low-altitude satellites pertinent to the study of the low-latitude boundary of the aurora, including both case studies and statistical treatments. The low latitude auroral boundary can be thought of as the low-altitude manifestation of convection boundaries for magnetospheric particles of moderate energy, although the detailed shape of the boundary might be modified locally by spatial variations or temporal modulation of precipitation rates. Several attempts have been made to compare observed equatorial and low-altitude boundaries with theoretical representations, with varying degrees of success. Here, the results of statistical analysis and case studies of the auroral boundary using precipitating particle data acquired by the NOAA spacecraft are presented. The ability of standard convection models to account for the observed boundary characteristics is discussed, with emphasis on the roles of convection strength and time dependence. It is demonstrated that, within reasonable parameter limits, steady-state convection patterns for moderate energy electrons generally fail to account for certain observed characteristics of boundary shapes. Further, it is demonstrated

20. DISTRIBUTION / AVAILABILITY OF ABSTRACT ☒ UNCLASSIFIED/UNLIMITED ☐ SAME AS RPT ☐ DTIC USERS	21. ABSTRACT SECURITY CLASSIFICATION Unclassified
22a. NAME OF RESPONSIBLE INDIVIDUAL	22b. TELEPHONE (Include Area Code) / 22c. OFFICE SYMBOL

DD FORM 1473, 84 MAR 83 APR edition may be used until exhausted
All other editions are obsolete.

SECURITY CLASSIFICATION OF THIS PAGE

UNCLASSIFIED

19. ABSTRACT (Continued)

that time-dependent transitions between various levels of activity can lead to characteristic boundary shapes that are quite dissimilar to steady-state solutions, and to some extent can provide a resolution between observed and computed boundary shapes for time scales pertinent to magnetospheric activity. The length of time after the onset of enhanced convection is found to be at least as important as the instantaneous level of activity as an ordering parameter for the shape of the low-latitude auroral boundary.

CONTENTS

FIGURES

1. INTRODUCTION

Many of the large-scale features of the spatial distribution of moderate energy charged particles in the magnetosphere can be understood in terms of steady-state convection due to a pervasive cross-magnetospheric electric field (Ref. 1). The details of charged-particle motion have been shown to depend on particle energy, charge, and pitch angle as well as the distribution of the convection electric field (Refs. 1 through 4). Southwood and Kaye (Ref. 5) have produced analytical relationships which are useful in studying the dependence of charged-particle trajectories on the particle characteristics and convection field model in steady state. Steady-state representations (Refs. 1, 4, 6) have been successful in describing in situ observations of the energy and spatial dependence of the plasma sheet inner edge (Refs. 7, 8), although it is recognized that the steady state must be at best a crude approximation to actual particle motion, which must be inherently time dependent.

Dynamic plasma injection processes have been studied extensively, and many phenomenological aspects of the injection processes are still somewhat controversial. Due to a wealth of data obtained recently from geosynchronous orbit, attention has focussed on specific features of the energy-time dispersion of particle injection events (Ref. 9). It is widely accepted that observed particle injection events can result either from the relative motion of spacecraft through a spatial structure embedded within a steady magnetospheric convection pattern (Ref. 8) or from actual time-dependent processes (Refs. 10, 11). Indeed, several distinct types of dynamic events can be identified in the data (Ref. 12) and several alternative concepts of the injection process have been proposed. These studies have contributed greatly to the identification and characterization of various manifestations of dynamic processes within the magnetosphere.

Here, it is proposed that certain general, large-scale features of the low-latitude boundary of the diffuse aurora, which is a manifestation of the plasma sheet inner edge (Refs. 13, 14), can be described best in terms of a time-dependent or "transition" state in much the same way as the shape of the plasmapause has been shown to exhibit strong time-dependent structure during periods of transition from quiet to disturbed conditions (Refs. 15, 16, 17).

Recent observations of electric fields and electron precipitation during the transition from quiet to active conditions have demonstrated some important large-scale features of auroral configurations which are inherently time-dependent. These include observations on the dayside of the disappearance of precipitation from the central plasma sheet for several hours following the onset of activity (Ref. 18). It is demonstrated that while the nightside auroral boundary responds uniformly and orderly to a transition from quiet to disturbed conditions, the dayside auroral boundary responds in a manner which is adverse to predictions deriving from steady-state representations. It is further demonstrated that the behavior of the nightside and dayside auroral boundaries, as determined from both statistical and case studies, can be represented by a simple time-dependent transition state which is a natural consequence of change in magnetospheric convection after the onset of activity. The length of time after the onset of enhanced convection is found to be at least as important as the instantaneous level of activity as an ordering parameter for the shape of the low-latitude auroral boundary. This latter conclusion could be important for global modeling efforts, since many empirical relationships used in modeling apply instantaneous values of activity indices such as Kp.

Similar time-dependent results have appeared implicitly in computer models of magnetospheric convection (Refs. 19, 20, 21, 22), and related ideas have been discussed qualitatively elsewhere (see, for example, Ref. 17). Here, a simple, quantitative numerical model is formulated which explicitly demonstrates systematic changes which occur in particle boundary topologies due to time dependence. While the numerical model used here is, in many ways, less robust than other models which have been applied to related problems, the model's simplicity aids in the isolation of the phenomenological features of interest in this work. Results of the modeling work are compared to observational data to further demonstrate important time-dependent aspects of the location of the equatorward boundary of the auroral zone. Due to the simplifying assumptions incorporated in the numerical model, no attempts to strictly simulate observed data are made.

II. OBSERVATIONS

Recently, extensive data sets have been acquired from charged-particle detectors on low-altitude polar-orbiting satellites concerning the low-latitude boundary of the diffuse aurora (see Ref. 14). The DMSP and NOAA satellites, in sun-synchronous orbits at 850 km altitudes, have provided especially useful data on precipitating auroral electrons. Each of the DMSP and NOAA spacecraft carries electron spectrometers which measure precipitating auroral electron fluxes from 30 eV to 30 keV on DMSP and from 300 eV to 20 keV on NOAA. The NOAA data have been used to compile statistical maps of the position of the low-latitude boundary of auroral electron precipitation as a function of magnetic local time, corrected geomagnetic latitude, and activity level (Ref. 23).

The auroral activity parameter chosen to order the NOAA statistical data set is an estimate of the power input to the polar regions by particle precipitation over the energy range 0.3 to 20.0 keV. This estimate is made directly from the particle observations acquired by the NOAA instrument during its pass over the polar region. In essence, the power input estimate is constructed by performing a line integral along the satellite trajectory of the observed precipitating energy flux, weighted by the cosine of the corrected magnetic latitude of the observation. A geometric conversion factor is applied to measurements from the individual polar passes to account for the manner in which the individual trajectories project into corrected geomagnetic coordinates. This procedure, which is performed to minimize the effects of magnetic dipole tilt on the computation of the activity levels, is described in detail in Ref. 24.

Over 60,000 orbits of NOAA data were used in the statistical study. The data were divided into nine levels of activity which progressed upward in a geometric fashion from the lowest (Level 1) which included power inputs below 2.5 gW to the highest (Level 9) which included power inputs between 60.8 and 96.0 gW. Level 5 in this sequence lay in the center of the distribution of power input values, and the average Kp during those NOAA orbits used to construct the Level 5 pattern was 2+ (see Ref. 24).

The equatorward boundaries of the auroral particle flux, defined as the lowest corrected geomagnetic latitude at which the energy flux exceeds 1.0 erg/cm^2 sec, are shown in Fig. 1 as a function of the auroral activity parameter based on precipitating particle power input. These equatorward boundaries are very well defined except in the noon to early afternoon magnetic local time sector where the average energy flux tends to fall below the 1.0 erg/cm^2 sec threshold at all latitudes. Also, the equatorward boundary location exhibits large variations (several degrees) about the average location a few hours either side of noon. On the nightside the typical variation in equatorward boundary locations for a given activity level is on the order of one degree about the average location. The statistical study was attempted using threshold values less than 1 erg/cm^2 sec for boundary identification, but the computerized boundary identification procedure tended to be unreliable at lower thresholds due to the spurious effects of low count rates and other background response at low latitudes.

The statistical boundary shapes are approximately circular in shape, offset toward midnight by several degrees, and, as expected, expand toward lower latitudes with increasing level of activity. These boundary shapes are similar to those reported in the study of Gussenhoven et al. (Ref. 14) which covered the evening (1600-2300 MLT) and morning (0400-1000 MLT) local time sectors. Here, the gaps near noon are due to an inability to identify the precipitation boundary due to consistently low flux levels ($<$ 1 erg/cm^2 sec) in the 12:00-14:00 local time range. In general, the boundary shapes for all levels of activity are similar, with the lowest latitude penetration occurring in the midnight sector. The auroral boundaries tend to be 10°-12° higher near noon than at midnight, and can be represented reasonably by offset circles in magnetic latitude and local time (see Ref. 25).

One must recall that the boundary shapes shown in Fig. 1 are based on a large number of samples of the aurora and do not represent, for example, the expected shapes that the auroral boundary might assume during a transition from quiet (e.g., Level 3) to disturbed (e.g., Level 9) conditions. Case studies are required in order to determine how the auroral boundary responds in time and space to the onset of enhanced activity. The results of one such case study, based on the combined data sets of the DMSP-F6, NOAA-7, and NOAA-8 spacecraft for a two-day interval, are presented in Figs. 2 and 3.

Figure 2 shows the hourly averaged auroral electrojet (AE) index and the 3-hour Kp index for the two day period which was chosen for study. The period from 12/9/83 to 12/10/83 was selected because of continuous data coverage for the DMSP and NOAA satellites and because the period contains a clear transition between an extended quiet period and an extended disturbed period. During the extremely quiet interval from 0300 UT on 12/9/83 to 0300 UT on 12/10/83, the AE index remained less than 30 gammas and the Kp index varied between 0 and 1. The 24-hour period on 12/9/83 was designated the Q1 day for December 1983 and was arguably the quietest extended interval in 1983. Activity increased slowly at about 0300 UT on 12/10/83 and increased more abruptly at about 0600 UT on 12/10/83. Conditions remained disturbed through most of 12/10/83, until a subsidence in activity occurred late on 12/10/83.

Figures 3a-d show the magnetic latitude of auroral boundary crossings in the dusk (15-21 MLT), midnight (21-3 MLT), dawn (3-9 MLT), and noon (9-15 MLT) local time sectors. While the DMSP-F6, NOAA-7, and NOAA-8 satellites are in nominal 0600-1800, 0300-1500, and 0900-2100 hour local time orbits, the earth's non-concentric spin axis and magnetic axis allows sampling of a large range of magnetic local times by these polar-orbiting spacecraft. Symbols indicate the spacecraft from which individual measurements were obtained. No distinction has been made between measurements in the northern and southern hemisphere. Boundary locations are plotted at the Universal Time and magnetic latitude at which precipitating electron flux levels were observed to cross a threshold flux of 0.10 erg/cm^2 sec. The plots cover the time period from 0600 U.T. on 12/9/83 to 2200 U.T. on 12/10/83. The onset of activity is marked at 0600 UT on 10/10/83, based on the sharp increase of the activity indices shown in Fig. 2.

The dusk auroral boundary remained near 70° magnetic latitude throughout the quiet interval and slowly propagated equatorward to about 58° latitude over several hours following the onset of activity. A recovery of the boundary back to 65° was observed late on 12/10/83. The scatter in the data points is due to small-scale variations in the auroral boundary over 2-3 hours of magnetic local time. For each individual measurement the local boundary position could be determined typically within 0.2° of latitude. The equatorward motion of the dusk auroral boundary is consistent with an average equatorward velocity of 0.03 km/sec. This boundary velocity is probably much lower than ambient convection speeds, which can exceed 1 km/sec during

disturbed times. Similar boundary motions were observed in the midnight and dawn sectors. The midnight auroral boundary propagated from 68° during the quiet period to at least 58° twelve hours after the onset of activity. Midnight data were not available during the period of maximum activity, so the total extent of propagation of the midnight boundary cannot be determined. The dawn boundary propagated from 69° during the quiet interval to about 57° twelve hours after the onset of activity. In each sector the average boundary motions were about one degree per hour.

The behavior of the auroral boundary in the noon sector was different from that observed in other local time sectors. During the quiet period the noon boundary resided between 70° and 72° magnetic latitude. Very low flux levels on the dayside during quiet times led to some uncertainty in identification of the boundary. Nevertheless, it was reasonably clear that the noon low-latitude auroral boundary initially moved to higher latitudes or even disappeared following the onset of activity before ultimately moving equatorward after about 12 hours. Between 0300 and 0600 on 12/10/83, the noon boundary moved from 70°-72° poleward to 75°-76°. After 0800 U.T., the noon boundary moved equatorward to about 63° magnetic latitude at 2000 U.T. Thus, the behavior of the noon auroral boundary is similar to that of other local times on time scales of 6-12 hours, but rather different on shorter time scales. It should be noted that the noon sector boundary values shown here attempt to depict the lowest latitude at which significant plasma sheet electron precipitation is observed. It is well known that precipitation in the noon sector can be attributed to a variety of sources, including the plasma sheet and the magnetospheric cusp (Refs. 26, 27, 28, 29). While the intention here is to depict the position of the plasma sheet boundary, some uncertainty is unavoidable at times of very low flux levels. Indeed, central plasma sheet precipitation has been reported to disappear altogether in the noon sector following the onset of activity (Ref. 18). If this were the case, some of the boundary values shown in Fig. 3 would be more indicative of the low-latitude boundary of the cusp during the time period from 0300 - 0900 UT on 12/10/83. Wherever possible, spectral characteristics were used to discriminate between electron precipitation from the plasma sheet and the cusp. However, flux levels and concomitant count rates tended to be too low (in the noon sector, from 0300-0900 UT) to produce reasonable energy spectra. For this reason, integral quantities such as energy flux were used

for the boundary analysis. The plotted boundary positions during this time interval should be regarded as lower limits for the plasma sheet boundary.

The expansion of the auroral oval seems to occur uniformly and directly on the nightside while it is delayed on the dayside and preceded by an initial poleward motion. About 3-12 hours after the onset of activity, the auroral boundary assumes a shape characteristic of the statistical representation of the active auroral boundary although equatorward boundary motion continues throughout the period of constant Kp on 12/10/83. Clearly, certain large-scale characteristics of the auroral boundary location depend not only on the instantaneous level of activity but also on the time history of the activity. The nightside sector (where, coincidentally, most auroral measurements are performed because of darkness requirements for optical viewing) responds most directly to instantaneous changes in activity. Also, the statistical results of Gussenhoven et al. indicate a better correlation between the auroral boundary location and the instantaneous value of the Kp index in the evening sector than in the morning.

III. ANALYSIS

It is intended here to investigate to what extent simple steady-state and time-dependent representations of auroral boundary shapes and motions can account for the major characteristics apparent in these observations. No attempt is made to specifically model the observational case study presented in this report, although it is hoped that a simple analytical representation can demonstrate the role of time dependence in determining large-scale configurations of auroral precipitation boundaries. Particle motion over large spatial scales in the magnetosphere is commonly treated under the constraints of conservation of energy and the first and second adiabatic invariants. Conservation of total energy (W) can be written

$$W = \varepsilon + q \left(E_c L^{\kappa} \sin \phi - \frac{\Phi_o}{L}\right) \tag{1}$$

where ε is the particle kinetic energy and q is the charge. The electrostatic potential energy consists of two components, the corotation potential (Φ_o = 91.5 kV) which scales inversely with radial distance (L, in earth radii), and the potential associated with the imposed magnetospheric convection. Here E_c is chosen so that the cross-magnetospheric potential drop at a prescribed distance equals a chosen value, and κ (=2) is chosen to provide partial shielding of the convection field at small radial distances from the earth. A value of κ = 1 represents a uniform electric field, although several authors have suggested that κ = 2 best represents conditions in the earth's inner magnetosphere (Refs. 30, 31, 32). In comprehensive numerical magnetospheric models shielding is implicit and time dependent, but for the purpose of this qualitative demonstration, shielding is treated parametrically using the Volland field model. The kinetic energy, under the constraints of constant first and second adiabatic invariants, is

$$\varepsilon = \varepsilon_o \left(\frac{L_o}{L}\right)^{\nu} \tag{2}$$

where ε_o is the particle kinetic energy at some reference distance L_o, and ν= 2 for magnetic field-aligned particles. For particles of intermediate

pitch equatorial angle (α_{eq}), Southwood and Kaye (Ref. 5) use the approximation

$$\nu \approx 2.1 + 0.9 \sin \alpha_{eq} \tag{3}$$

Particle motion based on these constraints lead to well-known characteristics which are demonstrated in Fig. 4. Figure 4 shows two examples of particle flow patterns for zero energy electrons in the equatorial plane over a range of ± 10 R_e radial distance from earth. The left panel of the figure shows the flow pattern for magnetospherically quiet conditions (50 eV cross-tail potential) and the right panel depicts disturbed conditions (200 kV cross-tail potential). In steady state, flow lines are equipotentials (dashed lines in Fig. 4) and the gradient of the potential is proportional to the flow velocity. The solid line in each panel depicts the separatrix or Alfven layer (e.g., Wolf, Ref. 22) between electron orbits which are open (i.e., extend from the tail to the noon "magnetopause") and those which are closed (i.e., corotating particles). The position of this boundary depends only slightly on particle energy in the energy range of interest for auroral studies ($\varepsilon \approx 1$ keV). This energy dependence is treated appropriately in later figures. For auroral studies, this boundary represents the closest approach of particles, whose origin is in the magnetotail, to the earth as a function of local time. Thus, the boundary would be manifested at low altitudes as the lowest latitude to which auroral electron precipitation could extend as a function of local time. The factor of 2 difference in penetration distance between quiet and disturbed conditions shown in Fig. 4 represents a change in the auroral boundary location from 66° magnetic latitude to 58° magnetic latitude at dusk. These values are quite representative of the observed positions of the auroral boundary under quiet and disturbed conditions, although no real attempt to match a specific set of observations is made here.

However, certain characteristics of the observed auroral boundary shape are not well represented by the results shown in Fig. 4. For example, the calculated auroral boundary is symmetric about the dawn-dusk meridian, implying that the auroral boundary at noon should lie at the same latitude as at midnight. Observations, on the other hand, show clearly that the noon low-latitude auroral boundary lies 10°-12° higher in latitude than the midnight boundary. Furthermore, the calculated auroral boundary penetrates to lowest

latitude in the dawn sector while observations indicate that the auroral boundary penetrates to the lowest latitude in the midnight sector.

Several effects can contribute to the offset of the auroral boundaries toward midnight. It is well known that the compression of the magnetosphere on the day side by the solar wind causes magnetic field lines at a given equatorial radial distance to map to a higher latitude at the earth's surface on the day side than on the nightside. This effect has been investigated analytically and observationally by several authors (Refs. 32, 33) for the poleward boundary of the auroral oval, where offsets of about 3-5° toward midnight can be expected. Somewhat smaller offsets of the equatorward boundary of the aurora due to this effect can be expected. This effect should be present even under steady conditions, and ample evidence exists for its presence, even in the earliest auroral data sets (e.g., Feldstein, Ref. 34). Also, apparent offsets of the equatorial auroral boundary can be caused by the erosion of particle flux as the particles experience precipitation loss while drifting from midnight toward noon. Precipitation losses lead to diminished particle flux throughout the auroral zone on the day side, and the same effect can cause the day side equatorial auroral boundary to appear much less sharp than on the night side. These observational features are apparent in the data set presented here even in steady conditions, and this effect caused some problems in identifying the day side boundary, as discussed earlier.

Some of the remaining discrepancies between the calculated and observed auroral boundaries could be overcome by modifying the convection electric field model in space and time. Indeed, it is probably the case that the real electric field distribution does not have the strict day-night symmetry present in the Volland field model. Convection models which are based on self-consistently calculated electric fields do show day-night asymmetries due to the closer penetration of the shielding layer on the night side than on the day side (see Ref. 22). However, these asymmetries would have to be quite severe to account for several aspects of the observed particle boundaries (in particular, the complete disappearance of plasma sheet particles in the noon sector). An alternative approach is to examine the behavior of the particle boundary during the transition between quiet and disturbed conditions. This investigation is presented here, with the expectation that the transition shape of the boundary might account for some of the major discrepancies be-

tween observations and a simple steady-state computation. A precedent for this type of study is the work done on the formation of plasmaspheric tails and detached plasma regions due to time-dependent convection effects (Refs. 15, 16).

One method of investigating the time-dependent evolution of the auroral boundary is to assume that the pre-existing, quiet, steady-state boundary (e.g., left panel of Fig. 4) experiences a step-function change in convection strength. The evolution of particle boundaries in the equatorial plane following a step-function change in convection strength is depicted in the various panels of Fig. 5. Figure 5 shows the boundary shapes for 1, 3, 6, and 12 hours after the onset of active conditions, as well as the ultimate steady-state solution. In each panel noon is at the top, midnight at the bottom, and dawn to the right. Boundary evolution is shown for three different electron energies; ε = 0, 1, and 10 keV. Conceptually and computationally, the ε = 0 boundary is straightforward since it simply represents the propagation of the pre-existing zero energy Alfvén layer, or plasmapause, in the new convection field (Ref. 15). It should be noted that particle boundaries are not equipotentials during the transition period between the initial and final steady states. The treatment of finite energy electrons is less straightforward since one must decide to what spatial location the kinetic energy pertains. For the purpose of this treatment it has been chosen to treat the energy as a "local" quantity. That is, the plots depict the regions of access of electrons with, say, 1 keV local energy, as though measurements were being made with spacecraft instruments, sensitive only to 1 keV electrons, at various positions in the equatorial plane.

The specific approach which was used to produce the time-dependent boundaries plotted in Fig. 5 is best described in terms of an example. In order to compute the configuration of the ε = 1 keV boundary for a time 1 hour following the onset of activity, a large set of "single particle" trajectories was computed. The single particle trajectories were computed using a disturbed electric field model (E_c = 5 kV/Re). The electron trajectories were initialized with ε_o = 1 keV with initial positions comprising a uniform dense grid in the equatorial plane (2,500 trajectories were computed with starting locations uniformly spaced between $-10\ R_e < X < 10\ R_e$, $-10\ R_e < Y < 10\ R_e$). Each of these 1 keV test particles was traced (backward in time) to determine

its position and energy at the time of onset of enhanced convection ($t = 0$). Each particle position and energy was then compared with the location of the Alfvén layer (for their appropriate energy at $t = 0$) under the pre-existing quiet conditions ($E_c = 1$ keV/R_e). Thus, the boundary for $\varepsilon = 1$ keV and $t = 1$ hour represents the spatial boundary between 1 keV electrons which would have traced back to a location at $t = 0$ which was internal to or external to a pre-existing Alfvén layer of appropriate energy. In this treatment no assumption is made about the distribution of "newly-injected" particles (c.f., Mauk and McIlwain, Ref. 11) other than their exclusion from the pre-existing Alfvén layer. It further represents a boundary between locations for which there is or is not a source for 1 keV electrons at a time one hour following the onset of enhanced convection. If, in the quiet initial steady state, finite energy electrons ($\varepsilon > 0$) only had access to those regions outside of the Alfvén layer (e.g., for a source in the earth's magnetotail) then electrons with $\varepsilon = 1$ keV could only be observed external to the boundary plotted in Fig. 5, for there would be no source for 1 keV electrons internal to the boundary. Note that the boundary itself is not "propagated," but rather the boundary is a manifestation of the location of 1 keV electrons relative to a pre-existing Alfvén layer at $t = 0$.

The clearest result of this analysis is the formation of an extension of the particle boundaries toward the dayside magnetopause within several hours of the onset of activity. At zero energy this result represents the formation of a dayside plasmaspheric tail, a feature which has been discussed by several authors (Refs. 15, 16) with regard to observations of detached plasma regions. Figure 5 shows that similar features develop for electrons of moderate energy and persist for several hours after the onset of enhanced convection.

The dayside tail eventually disappears and the boundary assumes its steady-state location after about 24 hours (topologically, the tail simply becomes thinner with time but never really disappears). Higher energy electrons have higher drift speeds and approach a steady-state configuration somewhat faster. At all energies the nightside portion of the boundary propagates inward toward the earth directly while the dayside boundary forms an extended tail which eventually becomes vanishingly thin. Pitch angle dependence is not important for very low energy electrons ($\varepsilon \leq 1$ keV) but can have

noticeable effects at energies near 10 keV. Particle boundaries for equatorially mirroring (solid lines) and magnetic field aligned (dashed lines) are plotted in Fig. 4. Pitch angle effects on the boundary configuration are most apparent on the dayside.

The results shown in Fig. 5 can be compared qualitatively to charged-particle observations in the equatorial plane. Fairfield and Viñas (Ref. 13) use data from the ISEE 1 charged-particle spectrometer to study the relationship between the inner edge of the plasma sheet and the configuration of the diffuse aurora boundary at low altitude. Their results indicate that the equatorial inner edge of the plasma sheet (at ε = 1 keV) at midnight typically resides near geosynchronous distance during quiet times but penetrates inward to about 3 R_e distance during disturbed times. In the 12-15 hour local time range, the plasma sheet inner edge is observed to occur outside of geosynchronous distance even during disturbed times. This result is qualitatively consistent with the formation of an extended boundary toward the dayside intervals such as those shown in Fig. 5. Possibly the final disturbed steady-state configuration is never achieved. Furthermore, the extreme scatter in the distribution of boundary data in Fairfield and Viñas seems indicative of the fact that the instantaneous activity index (Kp) does not order the boundary positions well.

The manifestation of the time-dependent boundary configurations in the low-latitude auroral boundary viewed from low altitudes is demonstrated in the series of plots in Fig. 6, which show boundary shapes projected into magnetic local time and magnetic latitude coordinates. For simplicity, a dipole field is used for these projections. The use of more realistic magnetic field models (e.g., Mead and Fairfield, Ref. 33; Fairfield and Mead, Ref. 35) would be required for specific comparisons with data, but would not lead to qualitatively different results. Again, similar to Fig. 5, the initial and final steady state solutions are shown in the left and right columns. The grids are drawn in 10° latitude increments with noon at the top and dawn to the right. The gap in the boundaries near noon indicate intersections with the dayside magnetopause which is taken to be at X = 10 R_e. The shape of these time-dependent boundaries on time scales of several hours has several features in common with observations. First, the dayside boundary resides at about 10° - 12° higher latitude than the nightside boundary, and second, the midnight

portion of the boundary responds most directly to the onset of activity. On the nightside the calculated boundary propagates to lower latitude at a rate of about 1° per hour, similar to observed rates. The similarity of the time-dependent boundary shapes for time scales of 3-6 hours to the statistical boundaries presented earlier and those of Gussenhoven et al. is quite strong.

Furthermore, the time evolution of the boundary as a function of local time also has characteristics similar to those of the case study presented earlier. Figure 7 shows the computed boundary location as a function of time for the dusk, midnight, dawn, and noon sectors. Note that the "quiet" and "disturbed" starting points are determined by an arbitrary choice of convection field strength, but of most importance is the expected qualitative behavior of the boundary during the transition period several hours following the onset of activity. The major features are that the dusk and midnight boundaries respond promptly and directly, and propagate equatorward at 1/2°-1° per hour for several hours while the dayside boundaries respond less directly. (Recall that the noon boundaries plotted in Fig. 3 represent lower limits in latitude.) The dawn boundary appears to respond with a 4-6 hour delay while the noon boundary responds by first propagating poleward by about 8°, then assuming a steady-state location after about one day. Over a two-hour local time sector near noon the boundary extends all the way to the dayside magnetopause. Aside from the delay in the response of the dawn boundary, each of these features is quite apparent in the observational case study results presented in Fig. 3. The strong similarity between the computed and observed boundary shapes is indicative of the importance of a simple, time-dependent transition state in determining auroral boundary locations.

IV. SUMMARY

Charged-particle detectors on low altitude satellites have acquired extensive data sets pertinent to the spatial and temporal behavior of the low-latitude boundary of the aurora. The results of a case study and an extensive statistical study of the auroral boundary using data from the DMSP and NOAA spacecraft are presented here. Major features of the observations are that the dayside low-latitude auroral boundary tends to reside about 10°-12° higher in latitude than the nightside boundary; the auroral boundary expands toward lower latitude with increasing levels of activity; and the noon boundary first propagates poleward or even disappears, then propagates equatorward following the onset of activity while the nightside boundary tends to propagate directly equatorward at a rate of ~ 1° per hour.

The low-latitude auroral boundary is the low-altitude manifestation of convection boundaries for magnetospheric particles of moderate (~ keV) energies. Steady-state representations of particle convection, based on conservation of energy and the first and second adiabatic invariants, can account for some of the basic features of the auroral boundary location and shape. However, several characteristics of the boundary shape cannot be represented by steady-state models without severe modifications of the convection field models. A simple time-dependent model based on the expected adiabatic response of the pre-existing auroral boundary to a step-function increase in convection strength can account for several large-scale observed characteristics of boundary location and motion. It is concluded that statistical representations of auroral boundary locations are best represented by a "transition" state of auroral boundary which is topologically dissimilar to steady-state representations. Further, it is concluded that the length of time after onset of enhanced activity is as important in ordering the configuration of auroral boundaries as the instantaneous level of activity.

REFERENCES

1. M. Alfvén and C.-G. Falthammar, Cosmical Electrodynamics, Oxford University Press, London (1963).

2. M. G. Kivelson and D. J. Southwood, "Approximations for the Study of Drift Boundaries in the Magnetosphere," J. Geophys. Res., 80, 3538 (1975).

3. D. P. Stern, "The Motion of a Proton in the Equatorial Magnetosphere," J. Geophys. Res. 80, 595 (1975).

4. S. W. H. Cowley and M. Ashour-Abdalla, "Adiabatic Plasma Convection in a Dipole Field: Electron Forbidden-Zone Effects for a Simple Electric Field Model," Planet, Space Sci., 24, 805 (1976).

5. D. J. Southwood and S. M. Kaye, "Drift Boundary Approximations in Simple Magnetospheric Convection Models," J. Geophys. Res., 84, 5773 (1979).

6. M. Ejiri, "Trajectory Traces of Charged Particles in the Magnetosphere," J. Geophys. Res., 83, 4798 (1978).

6. S. W. H. Cowley, "Energy Transport and Diffusion," in Proceedings of Solar-Planetary Environments, Vol. I., ed. by D. J. Williams, p. 582 (1976).

7. M. A. Schield and L. A. Frank, "Electron Observations Between the Inner Edge of the Plasma Sheet and the Plasmasphere," J. Geophys Res. 75, 5401 (1970).

8. W. J. Hughes, R. L. McPherron, J. N. Barfield, and B. Mauk, "A Compressional pc4 Pulsation Observed by Three Satellites in Geostationary Orbit Near Local Midnight," Planet Space Sci. 27, 821 (1979).

9. M. G. Kivelson, S. M. Kaye, and D. J. Southwood, The Physics of Plasma Injection Events," in Dynamics of the Magnetosphere, pp. 385-405, S.-I. Akasofu, editor, D. Reidel Publishing Company, Dordrecht, Netherlands, (1979).

10. S. E. Deforest and C. E. McIlwain, "Plasma Clouds in the Magnetosphere," J. Geophys. Res., 76, 3587 (1971).

11. B. H. Mauk and C. E. McIlwain, "Correlation of Kp with the Substorm-Injected Plasma Boundary," J. Geophys. Res., 79, 3193 (1974).

12. B. H. Mauk and C.-I. Meng, "Characteristics of Geostationary Particle Signatures Based on the 'Injection Boundary' Model," J. Geophys. Res., 86, 3055 (1983).

13. D. H. Fairfield and A. F. Vinas, "The Inner Edge of the Plasma Sheet and the Diffuse Aurora," J. Geophys. Res., 89, 841 (1984).

14. M. S. Gussenhoven, D. A. Hardy, and W. J. Burke, "DMSP-F2 Electron Observations of Equatorward Auroral Boundaries and their Relationship to Magnetospheric Electric Fields," J. Geophys. Res., 86, 768 (1981).

15. J. M. Grebowsky, "Time-Dependent Plasmapause Motion," J. Geophys. Res., 76, 6193 (1971).

16. H. A. Taylor, Jr., J. M. Grebowsky, and W. J. Walsh, "Structured Variations of the Plasmapause: Evidence of a Corotating Plasma Tail," J. Geophys. Res., 76, 6806 (1971).

17. C. R. Chappell, "Recent Satellite Measurements of the Morphology and Dynamics of the Plasmasphere," Rev. Geophys. Space Phys., 10, 951 (1972).

18. O. de la Beaujardiere, D. S. Evans, Y. Kamide, and R. Lepping, "Electric Fields and Particle Precipitation During the Substorm of January 18, 1984," submitted to the Proceedings of the Huntsville Workshop on Magnetosphere/ Ionosphere Plasma Models (1987).

19. P. H. Smith, N. K. Bewtra, and R. A. Hoffman, "Motions of Charged Particles in the Magnetosphere Under the Influence of a Time-Varying Large Scale Convection Electric Field," in Quantitative Modeling of Magnetospheric Processes, pp. 513-535, Geophysical Monograph No. 21, ed. W. P. Olsen, American Geophysical Union, Washington, D.C. (1979).

20. M. Harel, R. A. Wolf, P. H. Reiff, R. W. Spiro, W. J. Burke, F. J. Rich, and M. Smiddy, Quantitative Simulation of a Magnetospheric Substorm, 1. Model Logic and Overview, J. Geophys. Res., 86, 2217 (1981a).

21. M. Harel, R. A. Wolf, R. W. Spiro, P. H. Reiff, C.-K. Chen, W. J. Burke, F. J. Rich, and M. Smiddy, "Quantitative Simulation of a Magnetospheric Substorm, 2. Comparison with Observations," J. Geophys. Res., 86, 2242 (1981b).

22. R. A. Wolf, "Calculations of Magnetospheric Electric Fields," in Magnetospheric Physics, ed. B. M. McCormac, pp. 167-177, D. Reidel Publishing Company, Dordrecht, Netherlands (1974).

23. W. J. Hill, D. S. Evans, and W. M. Retallack, "A Near Real-Time Computer Display Showing the Geographic Location and Intensity of Auroral Precipitation Using the TIROS/NOAA Satellite Observations," EOS, 63, 1052 (1982).

24. J. C. Foster, J. M. Holt, R. G. Musgrove, and D. S. Evans, "Ionospheric Convection Associated with Discrete Levels of Particle Precipitation," Geophys. Res. Lett., 13, 656 (1986).

25. C. -I. Meng, R. H. Holzworth, and S. -I. Akasofu, "Auroral Circle Delineating the Poleward Boundary of the Quiet Auroral Oval," J. Geophys. Res., 82, 164 (1977).

26. R. H. Eather and S. B. Mende, "Airborne Observations of Auroral Precipitation Patterns," J. Geophys. Res., 76, 1746 (1971).

27. C. -I. Meng, "Electron Precipitation in the Midday Auroral Oval," J. Geophys. Res., 86, 2149 (1981).

28. P. -E. Sandholt, K. Henriksen, C. D. Deehr, G. G. Sivjee, G. J. Romick, and A. Egeland, "Dayside Cusp Auroral Morphology Related to Nightside Magnetic Activity," J. Geophys. Res., 85, 4132 (1980).

29. G. G. Sivjee and B. Hultqvist, "Particle and Optical Measurements in the Magnetic Noon Sector of the Auroral Oval," Planet. Space Sci., 23, 1597 (1975).

30. H. Volland, "A Semiempirical Model of Large-Scale Magnetospheric Electric Fields," J. Geophys. Res. 78, 171 (1973).

31. M. Ejiri, R. A. Hoffman, and P. H. Smith, "The Convection Electric Field Model for the Magnetosphere Based on Explorer 45 Observations," J. Geophys Res., 83, 4811 (1978).

32. S. -I. Akasofu, "A Study of Auroral Displays Photographed from the DMSP-2 and ISIS-2 Satellites," in Physics of the Hot Plasma in the Magnetosphere, edited by B. Hultqvist and L. Stenflo, p. 113, Plenum Press, New York (1975).

32. R. K. Jaggi and R. A. Wolf, "Self-Consistent Calculation of the Motion of a Sheet of Ions in the Magnetosphere," J. Geophys. Res. 78, 2852 (1973).

33. D. H. Fairfield and G. D. Mead, "Magnetospheric Mapping with a Quantitative Geomagnetic Field Model," J. Geophys. Res., 80, 535 (1975).

34. Y. I. Feldstein, S. I. Isaev, and A. I. Lebedinsky, "The Phenomenology and Morphology of Aurorae," Ann. IQSY, 4, 311 (1969).

35. G. D. Mead and D. H. Fairfield, "A Quantitative Magnetospheric Model Derived from Spacecraft Magnetometer Data," J. Geophys. Res., 80, 523 (1975).

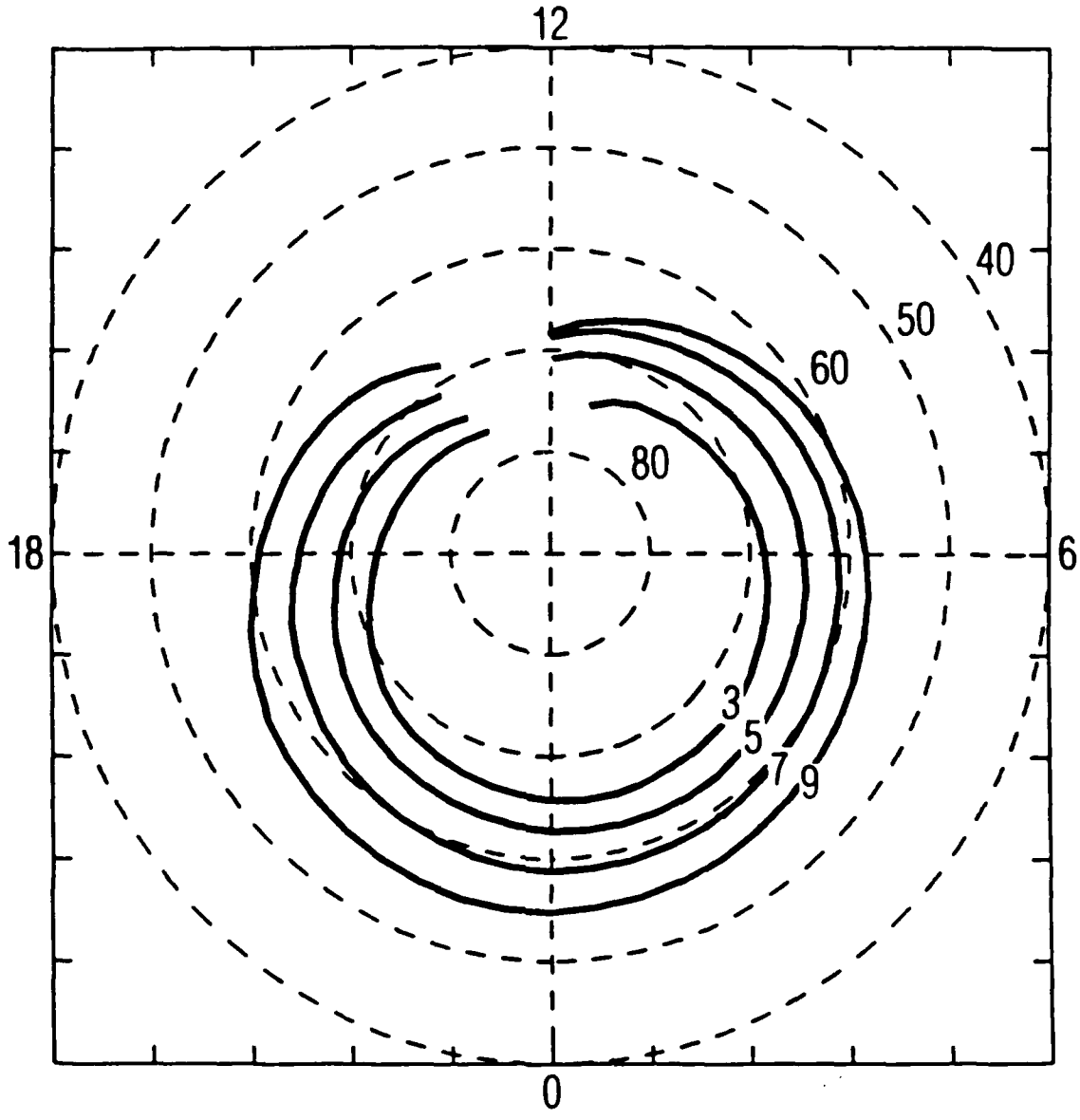

Fig. 1. Statistical Auroral Low-Latitude Boundaries Based on NOAA Charged-Particle Data, Plotted in Magnetic Local Time and Magnetic Latitude Coordinates. Boundaries are plotted for four levels of activity ranging from quiet (level 3) through disturbed (level 9).

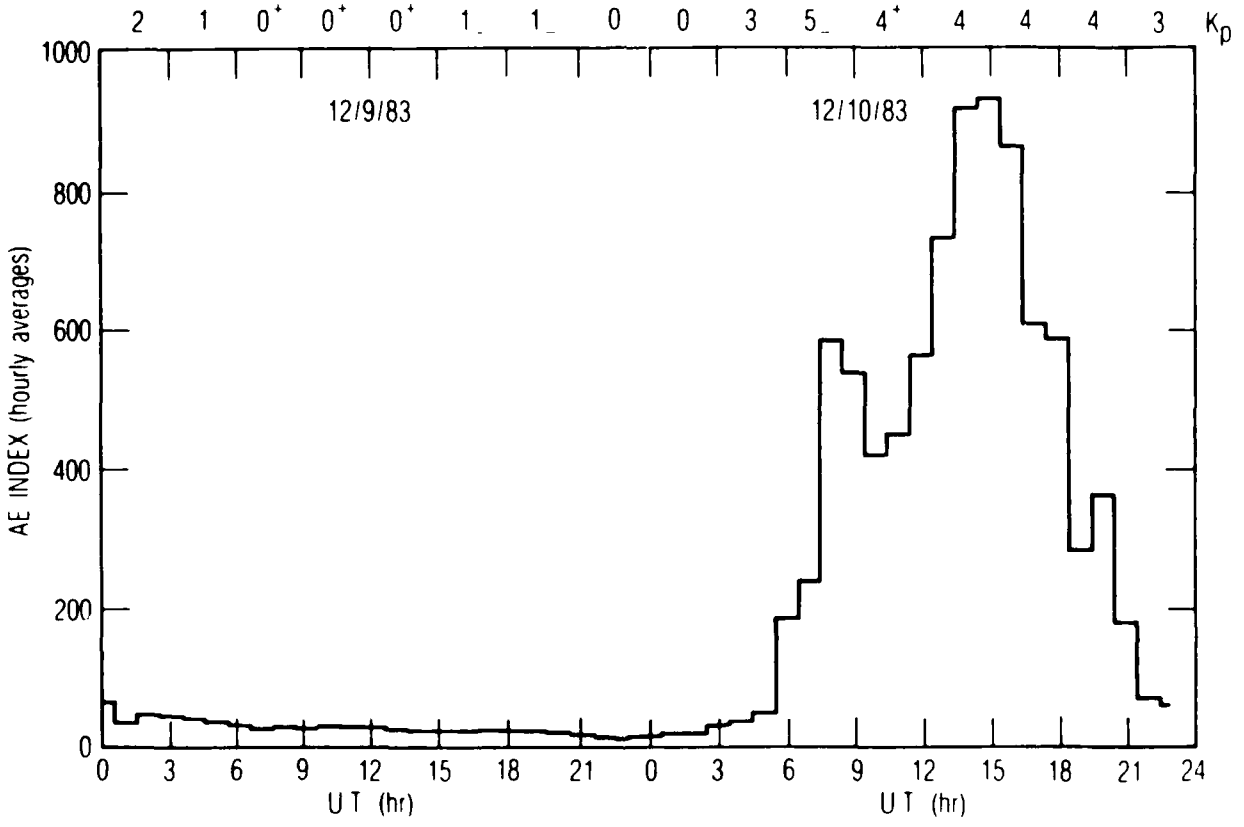

Fig. 2. Plot of the Hourly-Averaged AE Index and the 3-Hour Kp Index for the Two-Day Interval 12/9/83 - 12/10/83

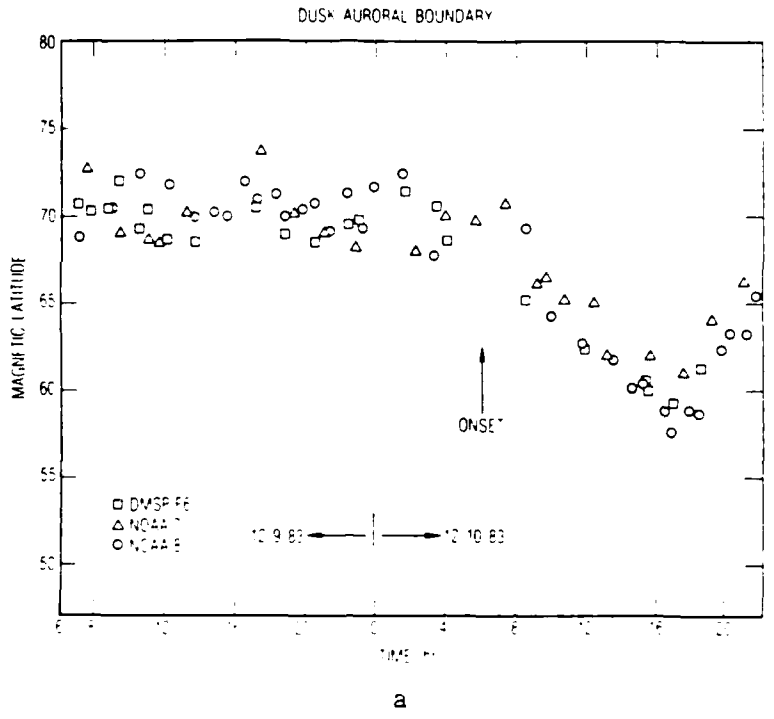

a

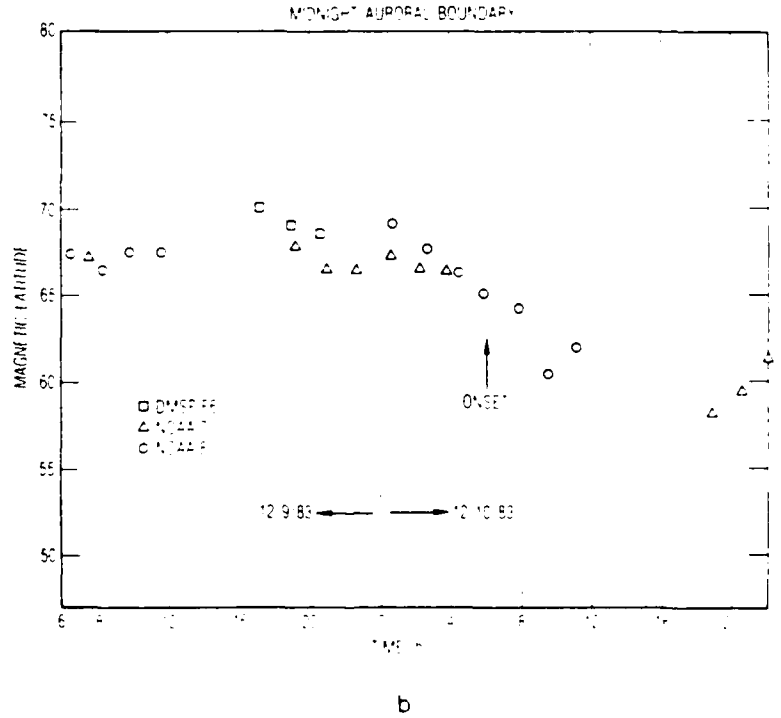

b

Fig. 3a-d. Plots of the Observed Position of the Low-Latitude Auroral Boundary as a Function of Time Based on Charged-Particle Data from DMSP-F6, NOAA-7, and NOAA-8. The period covered is from 0600 UT on 12/9/83 to 2200 UT on 12/10/83. An arrow marks the observed onset of activity at 0600 UT on 12/10/83.

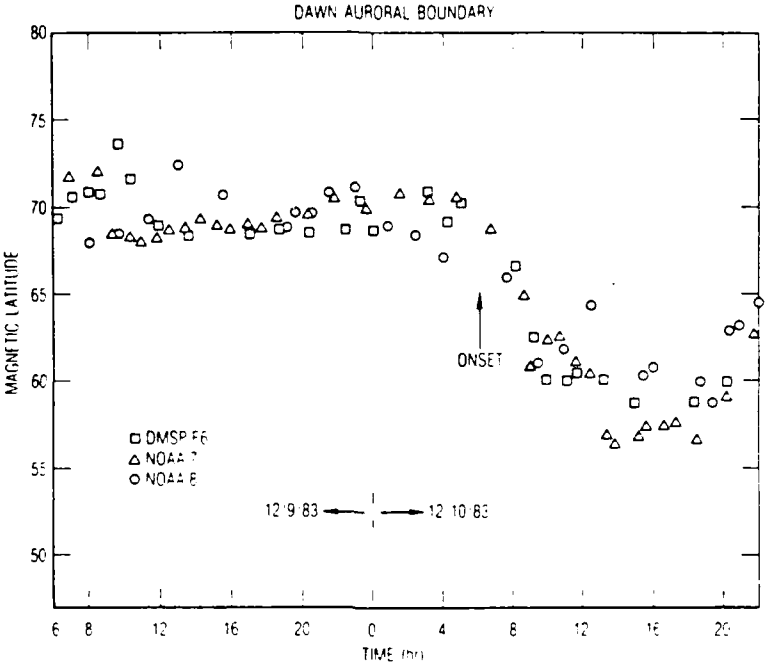
DAWN AURORAL BOUNDARY
MAGNETIC LATITUDE
80
75
70
65
60
55
50
ONSET
DMSP F6
NOAA 7
NOAA 6
12/9/83
12/10/83
6
8
12
16
20
0
4
8
12
16
20
TIME (hr)

c

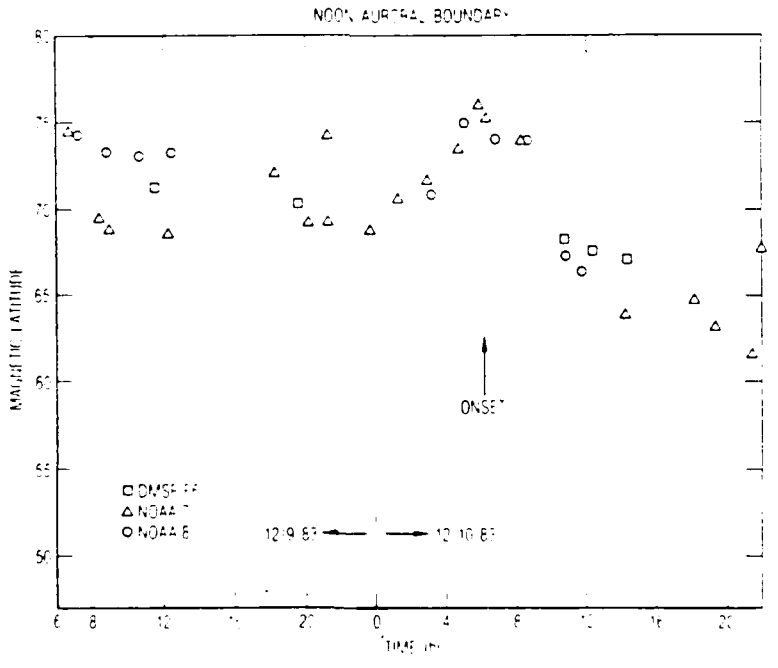
NOON AURORAL BOUNDARY
ONSET
NOAA 7
NOAA 6
12/9/83
12/10/83

d

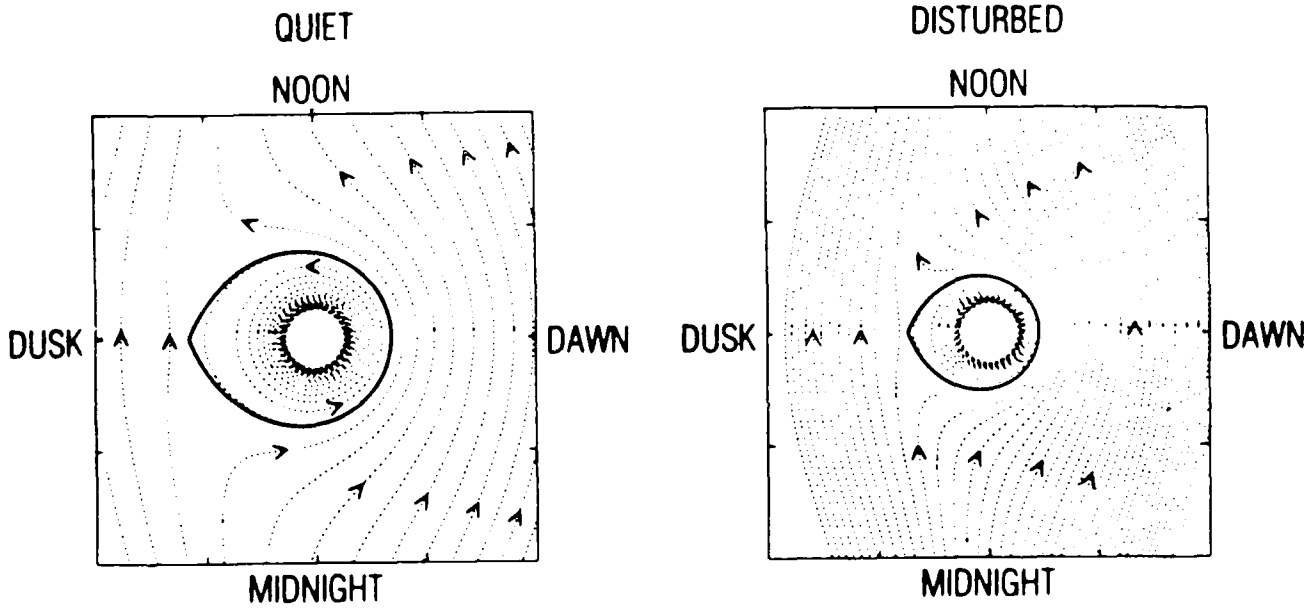

Fig. 4. Flow fields for Field-Aligned keV Electrons During Quiet and Disturbed Conditions. The spatial area covered is ± 10 earth radii in the geocentric equatorial plane. The solid line indicates the separatrix between open and closed drift paths.

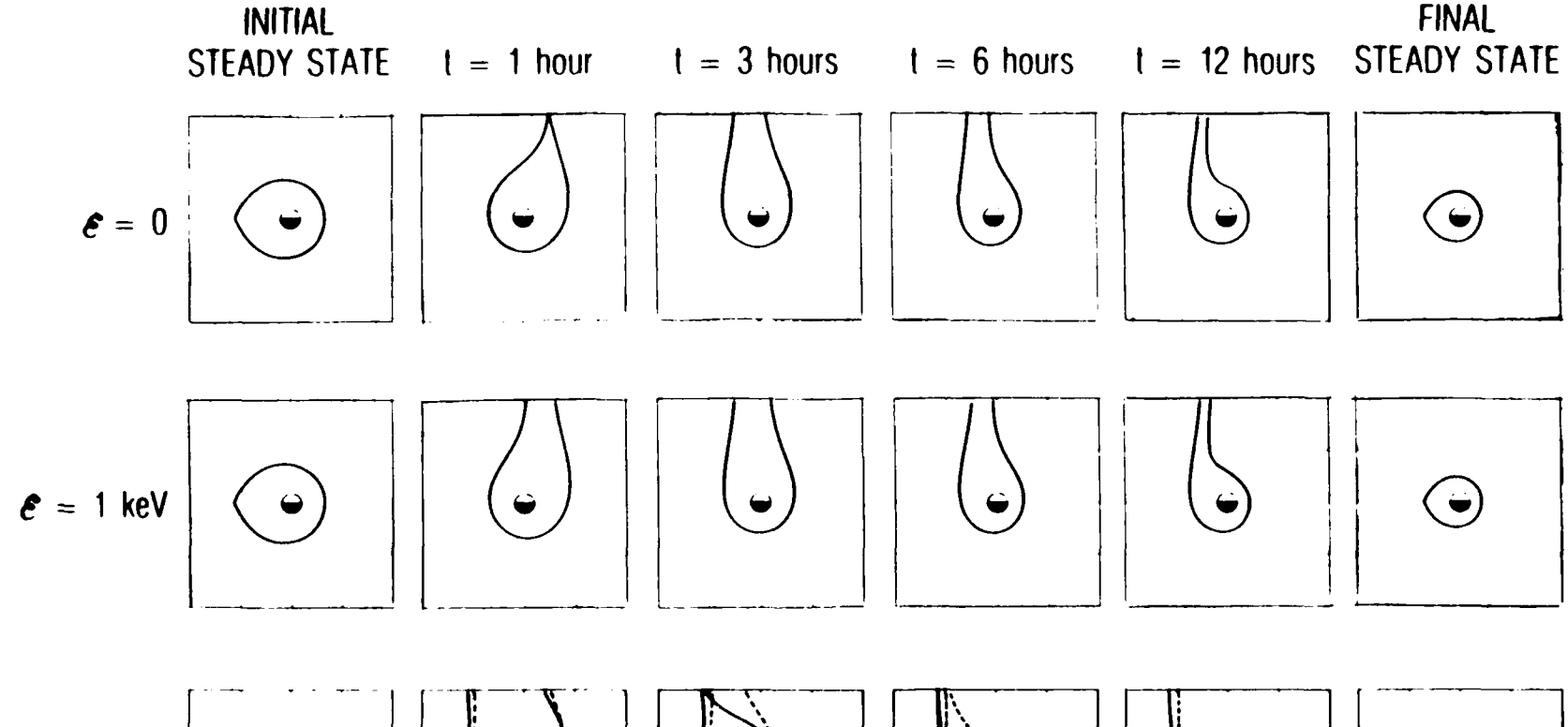

Fig. 5. Sequence of Plots Showing the Propagation of a Pre-Existing Quiet Auroral Boundary Following an Onset of Active Magnetospheric Convection. Noon is at the top and dawn is toward the right in each panel. Note that a long tail appears on the dayside and persists for several hours following the onset. Solid lines indicate boundaries for equatorially-mirroring particles and dashed lines indicate boundaries for field-aligned particles. Steady-state is assumed after about 24 hours.

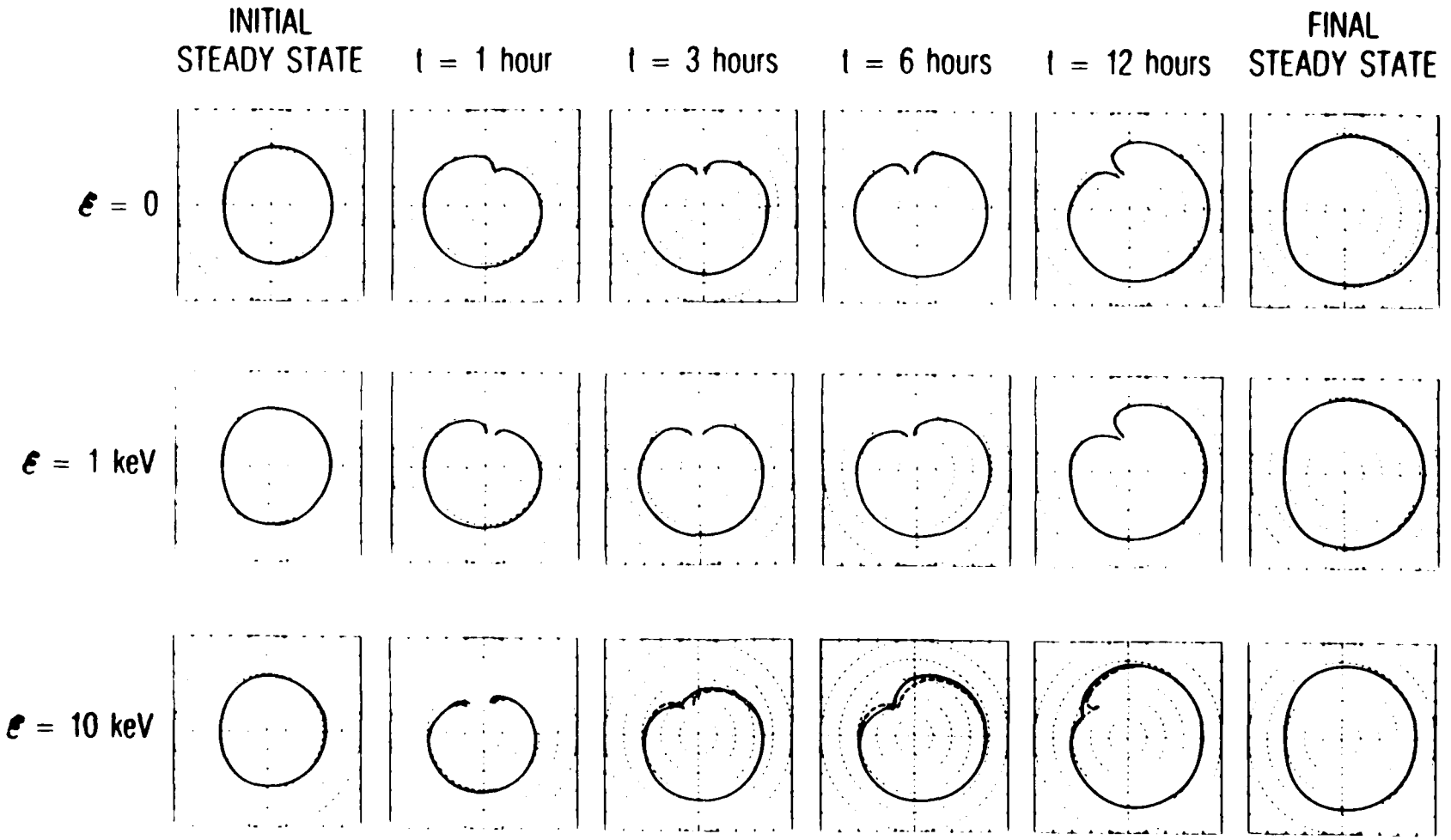

Fig. 6. Sequence of Plots in Magnetic Local Time and Magnetic Latitude Coordinates Showing the Propagation of the Low-Latitude Auroral Boundary Following the Onset of Activity. Noon is at the top of each panel and dawn is to the right. Latitude is shown in 10° increments. The thick solid line shows the auroral boundary in the "transition" state for equatorially-mirroring particles. Dashed lines indicate the boundaries for field-aligned particles. The open region on the dayside represents an intersection between the auroral boundary and the dayside magnetopause.

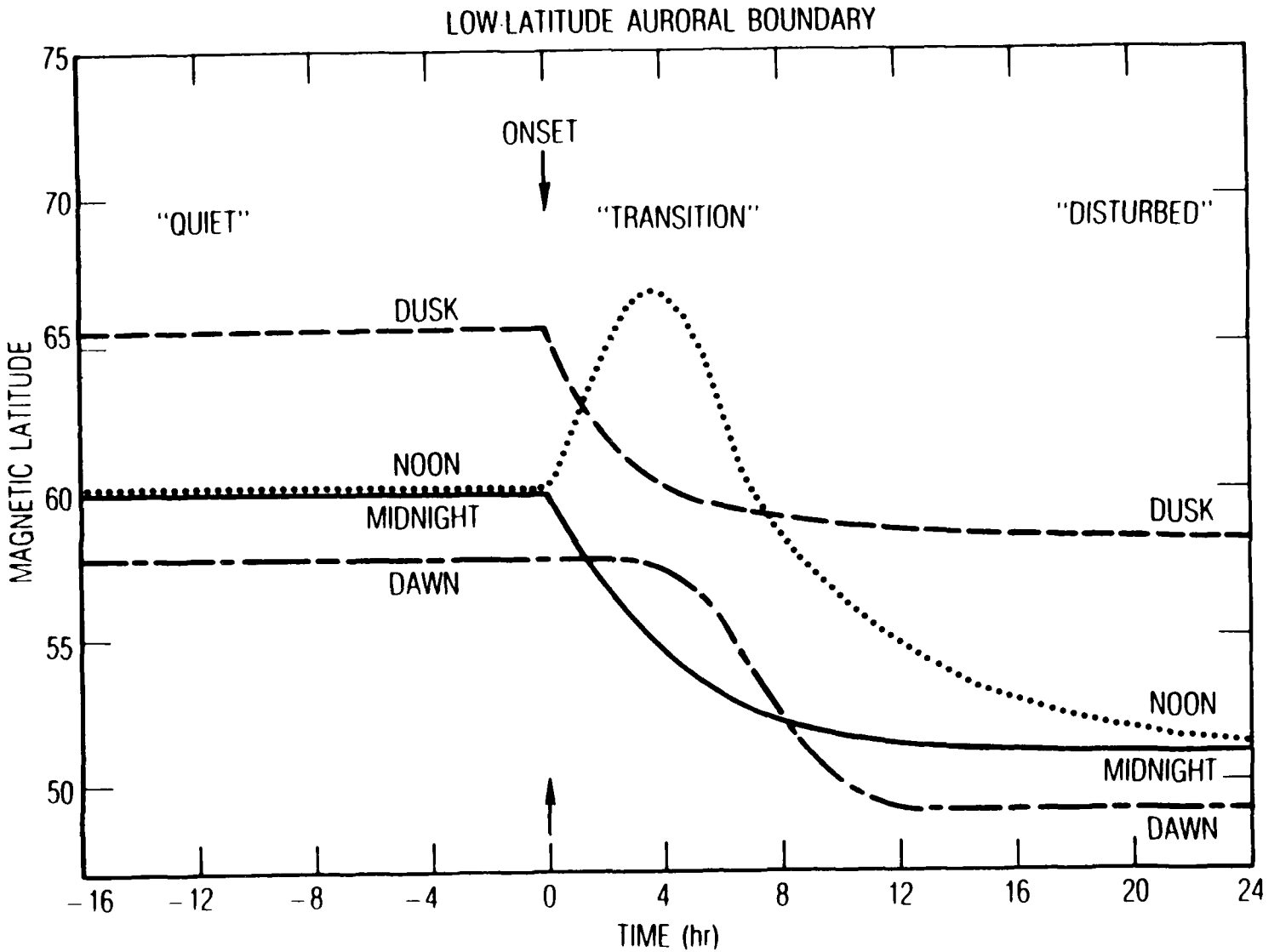

Fig. 7 Plot Showing the Temporal Evolution of the Auroral Boundary Location for Four Local Time Sectors. Note that the nightside boundaries propagate equatorward at about 1°/hour following the onset of activity while the dayside boundary propagates poleward then equatorward. Steady state is finally assumed after about 24 hours of activity.

LABORATORY OPERATIONS

The Aerospace Corporation functions as an "architect-engineer" for national security projects, specializing in advanced military space systems. Providing research support, the corporation's Laboratory Operations conducts experimental and theoretical investigations that focus on the application of scientific and technical advances to such systems. Vital to the success of these investigations is the technical staff's wide-ranging expertise and its ability to stay current with new developments. This expertise is enhanced by a research program aimed at dealing with the many problems associated with rapidly evolving space systems. Contributing their capabilities to the research effort are these individual laboratories:

Aerophysics Laboratory: Launch vehicle and reentry fluid mechanics, heat transfer and flight dynamics; chemical and electric propulsion, propellant chemistry, chemical dynamics, environmental chemistry, trace detection; spacecraft structural mechanics, contamination, thermal and structural control; high temperature thermomechanics, gas kinetics and radiation; cw and pulsed chemical and excimer laser development including chemical kinetics, spectroscopy, optical resonators, beam control, atmospheric propagation, laser effects and countermeasures.

Chemistry and Physics Laboratory: Atmospheric chemical reactions, atmospheric optics, light scattering, state-specific chemical reactions and radiative signatures of missile plumes, sensor out-of-field-of-view rejection, applied laser spectroscopy, laser chemistry, laser optoelectronics, solar cell physics, battery electrochemistry, space vacuum and radiation effects on materials, lubrication and surface phenomena, thermionic emission, photosensitive materials and detectors, atomic frequency standards, and environmental chemistry.

Computer Science Laboratory: Program verification, program translation, performance-sensitive system design, distributed architectures for spaceborne computers, fault-tolerant computer systems, artificial intelligence, microelectronics applications, communication protocols, and computer security.

Electronics Research Laboratory: Microelectronics, solid-state device physics, compound semiconductors, radiation hardening; electro-optics, quantum electronics, solid-state lasers, optical propagation and communications; microwave semiconductor devices, microwave/millimeter wave measurements, diagnostics and radiometry, microwave/millimeter wave thermionic devices; atomic time and frequency standards; antennas, rf systems, electromagnetic propagation phenomena, space communication systems.

Materials Sciences Laboratory: Development of new materials: metals, alloys, ceramics, polymers and their composites, and new forms of carbon; nondestructive evaluation, component failure analysis and reliability; fracture mechanics and stress corrosion; analysis and evaluation of materials at cryogenic and elevated temperatures as well as in space and enemy-induced environments.

Space Sciences Laboratory: Magnetospheric, auroral and cosmic ray physics, wave-particle interactions, magnetospheric plasma waves; atmospheric and ionospheric physics, density and composition of the upper atmosphere, remote sensing using atmospheric radiation; solar physics, infrared astronomy, infrared signature analysis; effects of solar activity, magnetic storms and nuclear explosions on the earth's atmosphere, ionosphere and magnetosphere; effects of electromagnetic and particulate radiations on space systems; space instrumentation.

...

END

DATE

FILMED

DTIC

JULY 88